Hydraulic jumps with corners due to obliquely inclined circular liquid jets

R. P. Kate, P. K. Das, and Suman Chakraborty*
Mechanical Engineering Department, Indian Institute of Technology, Kharagpur 721 302, India
(Received 6 February 2006; revised manuscript received 27 February 2007; published 22 May 2007)

We have discovered that hydraulic jumps corresponding to obliquely inclined circular liquid jets, under certain conditions of impingement, confer a series of interesting flow patterns (including jumps with corners). These patterns are markedly different from the regular elliptical (or oblate) shaped jump profiles that are commonly observed with higher angles of jet inclination. These patterns are attributed to the changes in the spreading flow profile due to "jet-jump interaction" at relatively lower jet inclination angles. The irregular shaped jump profiles, close to the critical angle of jet inclination, are mathematically characterized by introducing the concept of an equivalent jump radius. These theoretical predictions match excellently with the experimental findings. A phenomenological explanation is also provided by drawing analogies from shock-wave interactions in compressible fluid mechanics and from twin-jet interaction mechanisms.

DOI: 10.1103/PhysRevE.75.056310 PACS number(s): 47.20.−k

I. INTRODUCTION

Hydraulic jumps, in general, are the regions of rapidly varied fluid dynamic characteristics, connecting supercritical to subcritical free-surface or interfacial flows. Hydraulic jumps are typical to natural flows in rivers, channels, oceans, and spreading of impinging jets. Accordingly, discoveries on these phenomena find applications in various disciplines of science and engineering, ranging from atmospheric and oceanic sciences, chemical processing applications, impingement cooling, flood control systems, meteorological predictions, to even biofluidic sciences.

When a vertical circular jet of liquid hits a smooth horizontal surface, the fluid spreads out radially, as its vertical momentum is converted into horizontal momentum. Around an impingement zone, one notices a circular ring called the "circular hydraulic jump," where a discontinuity appears in the form of a sudden thickening of the fluid layer. These kinds of hydraulic jumps involve a strongly distorted free surface, a boundary layer region, and a subsequent separation of flow [1]. Such flow features have been studied extensively in the past, both theoretically [2–4], and experimentally [5–7]. Some other investigators [8–11] have addressed circular hydraulic jumps from a combination of theoretical and experimental perspectives, although the number of such studies reported has been very few. Watson [7], in a pioneering work, investigated the influence of viscous effects on the circular hydraulic jump and analyzed the flow in terms of a Blasius sublayer that is formed near the impingement point. In effect, he developed an expression for the location of the hydraulic jump, based on the Reynolds number at the impingement point and the liquid film thickness outside the jump, by employing linear momentum conservation principles. Brechet and Nèda [11] obtained scaling estimates for the radius of the jump, by taking the drop height (vertical distance of the nozzle tip from the plate) as an additional parameter, although the effect of the same on the jump radius turned out to be negligible in their study. Higuera [4] studied the circular hydraulic jump using a boundary layer approximation for the flow around the jump, and determined the position and structure of the jump numerically, by imposing pertinent boundary conditions at the edge of the plate. Bohr *et al.* [3] obtained detailed quantitative estimations for the location of the hydraulic jump, based on the flow rate and the viscosity of the liquid. In their analysis, they elaborated the viscous shallow-water theory of free-surface flows. They also obtained the jump locations, by an asymptotic matching of the flow behavior over regions upstream and downstream to the jump. The corresponding results were in good agreement with the experiments. Watanabe *et al.* [12] developed a simple quantitative method to describe different parts of the circular hydraulic jump, by studying laminar thin film flows with large distortions of the free surface. Bush and Aristoff [13] analyzed the influence of surface tension on laminar circular hydraulic jumps through a detailed mathematical modeling. However, their experiments revealed that the influence of surface tension on the jump radius turns out to be rather marginal, and can therefore be neglected for the laboratory scale jumps under consideration.

Normal impinging jets have been found to give rise to various complicated jump patterns as well, other than the trivial circular ones. For instance, Ellegaard *et al.* [14], in their experiments on normal impinging jets, observed that at a particular rim height, the circular hydraulic jump undergoes a spontaneous breaking in the azimuthal symmetry and assumes a stationery polygonal shape. Several stationery polygons could be observed by them at the same flow parameters. A few researchers offered with theoretical insights related to the formation of these kinds of irregular shaped jump profiles with normal impinging jets. Putkaradze and Dimon [15] showed that the nonuniformity of flow along the radial direction, at the corners of the polygonal shaped jump profiles, can be captured by including the viscous terms in the cross-radial component of the momentum conservation equation. More recently, Aristoff *et al.* [16,17] revealed a new series of steady asymmetric jumps with striking shapes such as cats eye, three- and four-leaf clovers, sunflowers, bowties, and butterflies.

*Corresponding author.
Electronic address: suman@mech.iitkgp.ernet.in

Unlike the hydraulic jumps formed as a consequence of normal impinging jets mentioned as above, hydraulic jumps associated with oblique impinging jets are inherently asymmetric in nature. Consequently, the stagnation point location in the impingement zone, which is conventionally considered to be a source of the radially spreading flow, is not coincident with the geometrical center of the jet for an oblique jet inclination. An upstream shift of the stagnation point from the geometrical center of the noncircular impingement zone, for oblique impinging jets, has been reported by various investigators over the past few decades [18–23]. Kate *et al.* [23], in a recent investigation, analyzed the noncircular hydraulic jumps formed as a consequence of oblique impingement of circular liquid jets on a stationery flat horizontal plate, both from experimental and theoretical perspectives. Their studies suggested that the "regular" oblate shape of the jump profiles are likely to be disturbed and distorted considerably, in case the angle of obliquity of the jet impingement is progressively decreased. Such cases, however, were not elaborated and theoretically addressed in the above-mentioned study.

It is also interesting to note here that another typical class of oblique impinging jet studies, characterized by the formation of irregular shaped patterns that closely resemble the jump profiles with corners formed due to single impinging jets, deals with the oblique collision of two jets. Under these conditions as well, the axisymmetry of the facing configuration is eventually lost [24–29].

II. JET-JUMP INTERACTIONS FOR SINGLE OBLIQUE IMPINGING JETS: IRREGULAR-SHAPED JUMP PROFILES

The aim of the present study is to elucidate the mechanisms of the formation of certain irregular and nonintuitive shapes of hydraulic jump profiles, originated as a consequence of oblique impingement of single circular liquid jets on a flat horizontal plate. In order to assess the situation from a fundamental geometrical perspective, it can be noted here that the impingement zone of an obliquely impinging jet of radius r_0, inclined at an angle ϕ (with the horizontal) with a flat horizontal plate, turns out to be an ellipse of major axis $r_0/\sin\phi$. The shift of the stagnation point from its geometrical center is nothing but the distance $r_0 \cot\phi$ (refer to Fig. 1). The volume flux distribution $\psi(\phi,\theta)$ of the radially spreading flow (where θ is the polar angle specifying the location of the point in the plane of the plate, with reference to the stagnation point) can be given as [26]

$$\psi(\phi,\theta) = \frac{r_0^2 V}{2} \frac{\sin^3\phi}{(1+\cos\phi\cos\theta)}, \tag{1}$$

where V is the velocity of the impinging jet. Consequently the radial locations of the jump, $R(\phi,\theta)$, can be obtained as [23]

$$R(\phi,\theta) = C\psi^{5/8}\nu^{-3/8}g^{-1/8}. \tag{2}$$

It is important to mention here that the expression given by Eq. (2) follows directly from a detailed scaling analysis of the continuity and the momentum conservation equations.

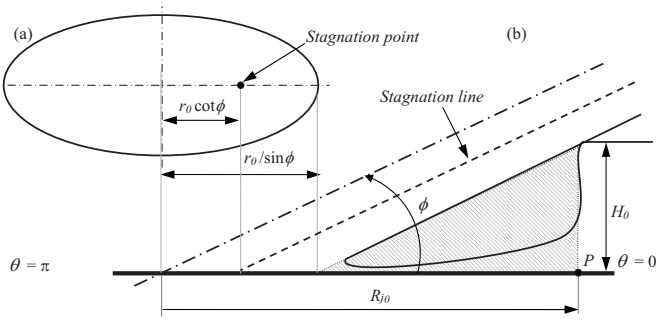

FIG. 1. A schematic of jet jump depicting the geometrical features of the noncircular hydraulic jumps formed due to oblique impinging jets. A typical jump-jet interaction is illustrated in the figure.

Taking V_r^* and V_z^* as the characteristic scales for the radial and axial velocity components, R^* as the characteristic scale for the jump radius, and h^* as the characteristic film thickness, it is possible to obtain appropriate scaling estimates of the local jump radius and the corresponding film thickness. To achieve this purpose, an order of magnitude analysis may be executed by combining the continuity and the linear momentum conservation equations, to yield $\frac{V_r^{*2}}{R^*} \sim \frac{gh^*}{R^*} \sim \frac{\nu V_r^*}{h^{*2}}$, which is nothing but an expression for dynamic balance between the inertia, gravity, and viscous forces. This scaling estimation is essentially coupled with the constraints of overall mass balance at specified azimuthal and polar locations [i.e., $r\int_0^h V_r(r,z)dz=\psi$], to result in the following: $R^* \sim \psi^{5/8}\nu^{-3/8}g^{-1/8}$ and $h^* \sim \psi^{1/4}\nu^{1/4}g^{-1/4}$. A combination of these expressions reveals that the jump radius and the film thickness, indeed, are implicitly related. This implicit relationship can be written in the following mathematical form: $R=R[h(\psi,\upsilon,g)]$. However, prescribing the radial location of the jump as an explicit function of the film thickness is not a practically realizable proposition for the present study, since the film thickness is not independently varied during our experiments. Rather, the local film thickness evolves as an explicitly dependent function of the local volumetric flow rate, gravitational acceleration, and the kinematic viscosity. Based on these considerations, many of the research investigators on hydraulic jumps, with their experimental arrangements similar to ours, have preferred to describe the evolution of jump radius and film thickness as two separate parametric functions of the same set of variables (namely, ψ,υ,g), rather than treating the film thickness as an independently controllable parameter (for example, please refer to [11,12]).

It is also important to recognize here that the radius of the circular hydraulic jump can be obtained from Eq. (2) as a special case when $\phi=90°$. Under this condition, volume flux distribution can be obtained as

$$\psi = \frac{r_0^2 V}{2} = \frac{Q}{2\pi}. \tag{3}$$

Hence it can be observed that the radial location of the hydraulic jump, both for the circular and noncircular oblate shaped jumps, is a function of volume flux distribution only.

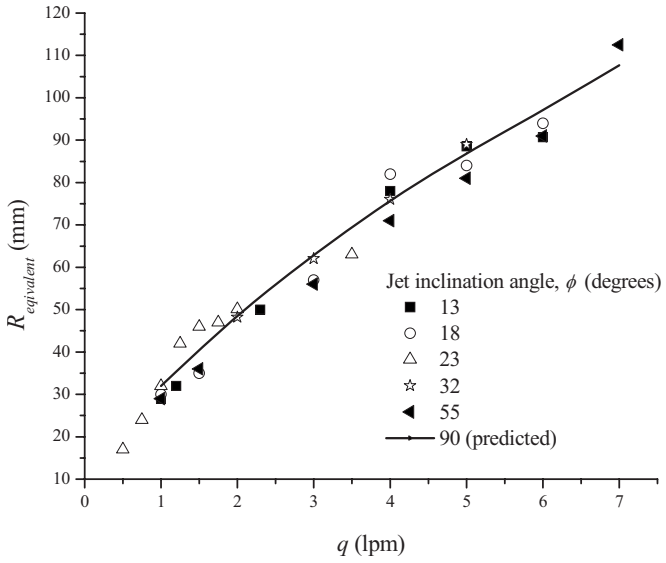

FIG. 2. Radius of the equivalent circular hydraulic jump for different jet inclination angles as a function of volume flow rate of water.

However, locations of the hydraulic jumps with corners (jumps obtained when jet inclination angle $\phi \leqslant 25°$ (critical jet impingement regime) cannot be obtained directly from Eq. (2). For these cases (jumps with corners), we first measure the area bounded by the jump profile A_j. Subsequently, these jump profiles are expressed in terms of an equivalent jump radius $R_{equivalent}$ (based on an equivalent circular jump profile with the same area as that bounded by the irregular shaped profile in the onset of the instability), given as

$$R_{equivalent} = (A_j/\pi)^{1/2}. \tag{4}$$

A typical plot of $R_{equivalent}$ as a function of q $(=Q/2\pi)$, very much analogous to the corresponding plots for regular-shaped jumps [23], is depicted in Fig. 2. The plot also includes $R_{equivalent}$ for regular (oblate) shaped jumps obtained under the condition $25° \leqslant \phi < 90°$. As can be demonstrated from Fig. 2, these scaling predictions are somewhat universal, and match quite well with the experimental outcome, in an order of magnitude sense for jump profiles of disparate shapes (circular hydraulic jumps, jumps bounded by smooth curves, and also jumps with corners).

From the previous analysis, it is also apparent that the liquid "thin film" thickness $h(\phi, \theta)$ just upstream of the jump locations can be obtained as

$$h(\phi, \theta) = C\psi^{1/4}\nu^{1/4}g^{-1/4}, \tag{5}$$

where C is a constant, depending on the velocity profile chosen, ν is the kinematic viscosity of the liquid, and g is the acceleration due to gravity. It is interesting to note that as the nozzle inclination becomes more acute, there is likely to be a direct contact of the upstream apex of the jump profile ($\theta = 0$) with the impinging jet (depending on the jet diameter). We term this confluence as jump-jet interaction, and first theoretically obtain a condition for the critical angle of jet inclination (ϕ_{critical}) leading to an onset of this phenomenon.

A. Critical condition for jump-jet interaction

In order to assess the conditions for the onset of jump-jet interactions, one may first note that for steady-state flow, the resultant thrust must be zero at the jump. In other words, the momentum flux through a surface at the jump is nullified by the force due to pressure differentials on the downstream side of the same. Assuming H to film thickness just downstream of the jump location, the balance of linear momentum across the jump can be mathematically expressed as

$$\frac{1}{2}g(H^2 - h^2) = \left(\frac{\psi}{R_j}\right)^2\left(\frac{1}{h} - \frac{1}{H}\right). \tag{6}$$

When $h \ll H$, this reduces to

$$\frac{1}{2}gH^2 = \left(\frac{\psi}{R_j}\right)^2\left(\frac{1}{h}\right). \tag{7}$$

Since the jet-jump interaction is instigated at the location of the jump at $\theta = 0$, the corresponding height of the jump at $\theta = 0$ can be written as

$$H_0 = \left(\frac{2}{gh_0}\right)^{1/2}\frac{\psi_0}{R_{j0}}, \tag{8}$$

where the subscript "0" indicates the value of the respective quantities at $\theta = 0$. Now, for the jet-jump interaction to take place, one can write (from the shaded triangle in Fig. 1)

$$H_{critical} = R_{j0}\tan\phi_{critical} - \frac{r_0(1 - \cos\phi_{critical})}{\cos\phi_{critical}}. \tag{9}$$

The critical angle of jet inclination, ϕ_{critical}, for a jet of radius r_0 and velocity V, can thus be obtained by equating H_0 with $H_{critical}$, as

$$R_{j0}\tan\phi_{critical} - \frac{r_0(1 - \cos\phi_{critical})}{\cos\phi_{critical}} = \left(\frac{2}{gh_0}\right)^{1/2}\frac{\psi_0}{R_{j0}}. \tag{10}$$

B. Experimental studies: Transition from regular shaped jump profiles to irregular shaped ones

In order to validate the above-mentioned estimate, as well as to elucidate the jump profiles formed beyond the critical angle of jet obliquity, we have performed a series of laboratory experiments on hydraulic jumps with oblique impinging jets. A typical experimental setup consists of a closed loop system consisting of a nozzle through which water impinges on a flat horizontal glass plate of dimensions 1×1 m and thickness 10 mm mounted on four leveling screws. A centrifugal pump (0.5 HP, head 30/6 m, capacity 15/40 lpm, 2800 rpm) is used for delivering filtered water in the form of a jet at the required flow rate. The flow rate is measured using two rotameters calibrated in the range of 1–10 and 1–20 lpm. Circular tubes of brass and stainless steel, in the diameter range 4–10 mm, are used as nozzles. These nozzle tubes have length to diameter ratio of 150 to 200 to ensure a fully developed flow at the exit. The edges of the glass plate are chamfered with a radius of approximately 4 mm on both

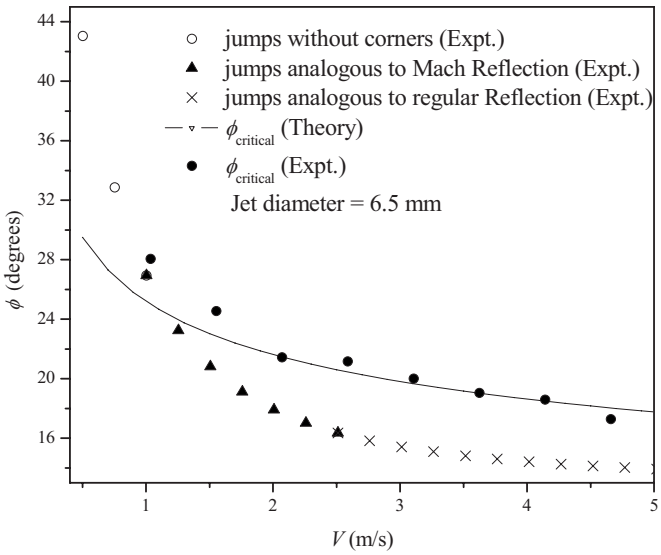

FIG. 3. Critical value of jet inclination angle required for jump-jet interaction.

top and bottom faces for the smooth drainage of liquid. Arrangements are made to adjust the distance of the nozzle from the plate in the range 0–50 cm. The jet impinging on a flat horizontal plate spreads radially and then falls freely from the edge of the plate into a collecting reservoir. The jet angle (ϕ) can be calculated from the nozzle angle (ϕ_n) and jet velocity (V) as

$$\phi = \tan^{-1}\left(\frac{\sqrt{V^2 \sin^2 \phi_n + 2gH}}{V \cos \phi_n}\right), \tag{11}$$

where H is the vertical distance of the center of the nozzle tip from the target plate. As the angle of jet inclination, ϕ, marginally deviates from the critical angle of obliquity defined by Eq. (10), radially asymmetric oblate shaped jump profiles are initially observed. A set of critical values of the jet inclination angle, as obtained from our experiments under different flow conditions, is depicted in Fig. 3. These observations agree well with the corresponding theoretical estimations predicted from Eq. (10). With further lowering of the jet inclination angles, a series of jump profiles with altogether different shapes emerge. Jump profiles under these conditions have one or more corners. At lower values of the jet velocity, the jump profile assumes more or less a triangular shape. With further increases in the jet velocity, the relatively straight bases of the triangular jump profiles turn out to be of bowed shape. At a particular velocity of the jet, the base totally disappears and a "jump-jump intersection" is observed at the downstream apex of the jump profile.

C. Analogy with shock wave interactions

The irregular shaped hydraulic jump profiles discovered by us can be fundamentally explained by drawing analogies with shock wave interactions. In fact, the resemblance between the shooting flow of an incompressible fluid and supersonic compressible fluid flow has been topic of interest for many years [29–32]. It is important to note in this context

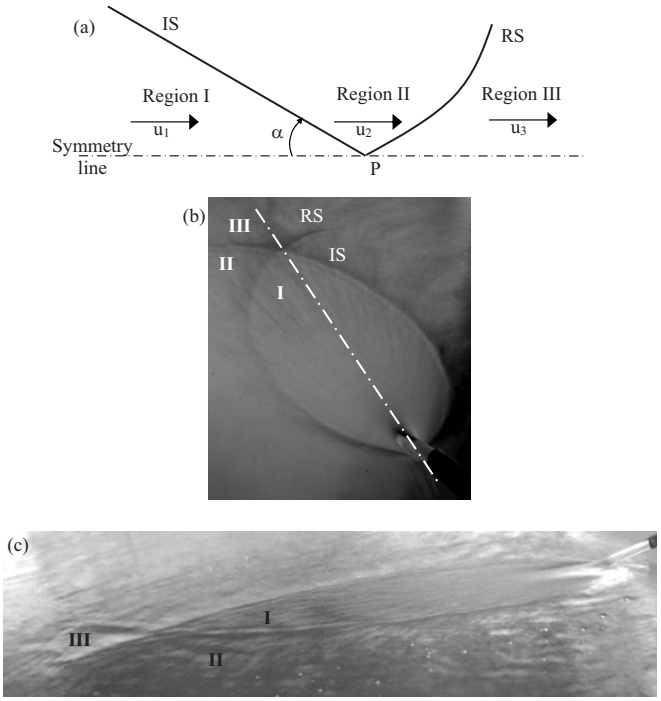

FIG. 4. (a) Regular reflection; (b) and (c) hydraulic jumps analogous to regular reflection.

that in case of compressible fluid flows, two types of reflection waves are possible, namely, the regular and Mach reflection waves. In the first case (see Fig. 4), a reflected shock wave (RS) is formed at the intersection point of the incident shock, (IS), and a plane rigid wall. It could as well refer to the intersection of two equal straight shocks, where the wall becomes the plane of symmetry. The fluid with velocity u_1 in the region I approaches the incident shock. As the fluid passes through this shock, it is slowed down and deflected to a velocity u_2 in region II. The reflected shock (RS) deflects the flow from the velocity u_2 to a velocity u_3 in region III. The deflected flow must be parallel to the boundary wall or to the plane of symmetry. It is also important to note here that when a fluid with a speed $U > c$ (characteristic wave speed) impinges normally onto an obstacle, a normal shock forms and propagates in the U direction. If, instead, the fluid velocity and the obstacle are not perpendicular to each other, an oblique shock forms and propagates into the flow at an angle and with a speed that can be determined by the local flow rates [31,33].

Our experimental observations reveal that hydraulic jump profiles, analogous to regular reflection waves in compressible fluid flows, indeed occur for angles of jet inclination less than $\phi_{critical}$, corresponding to the pertinent jet velocity. These jump profiles are observed in conjunction with jump-jet interactions occurring at the extreme apex of the jump profile and the jump-jump intersections at the extreme base of the same. Due to a confluence of the jet and the jump, a jump in upstream flow is not visible. As a consequence, it becomes impossible to locate the exact jump location at this point. In absence of the jump-jet interactions, on the other hand, the impingement zone can be considered to be of an elliptic shape from simple geometrical considerations. The

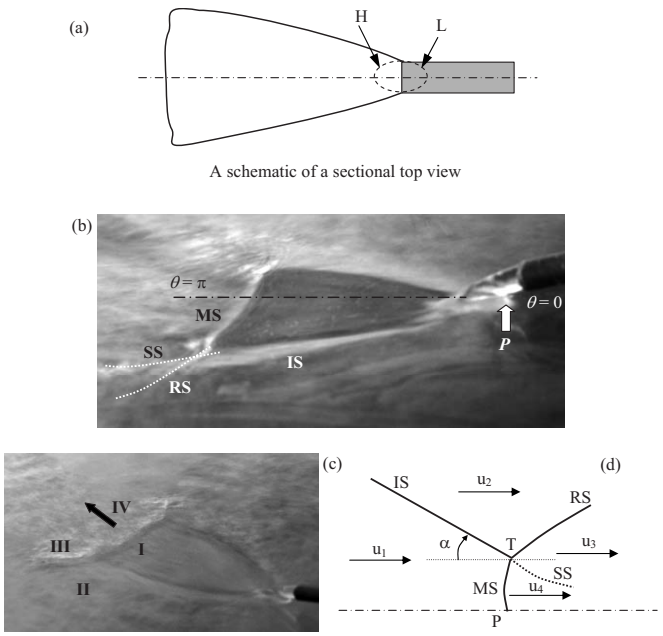

FIG. 5. (a) Mach reflection; (b)–(d) hydraulic jumps analogous to Mach reflection.

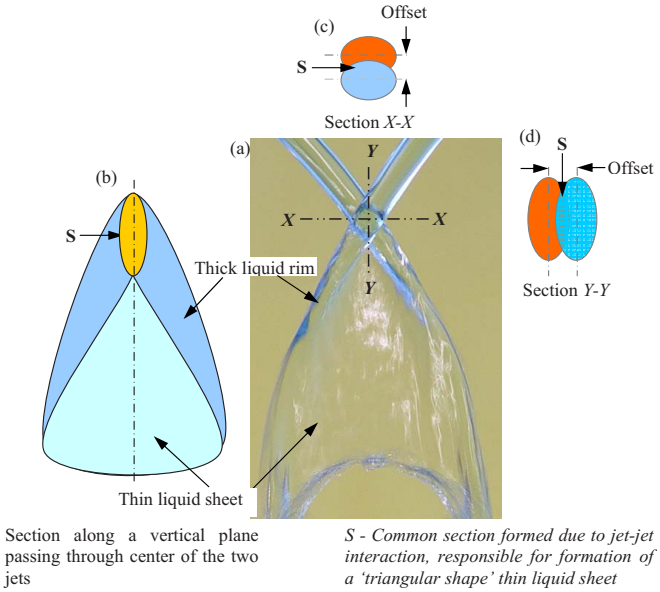

FIG. 6. (Color online) Triangular liquid sheet formation due to partial oblique collisions of two circular liquid jets.

jump-jet interaction, in effect, perturbs the elliptic shape of the impingement zone and the resulting flow field. Analogous to regular reflections, it is observed from our experiments that the radial flow approaching the curved incident shock is slowed down and gets deflected, and remains more or less radial as it crosses the jump. The flow in region III, however, turns out to be unidirectional and is parallel to the line of symmetry, as depicted in Fig. 4.

When the incident shock is too strong and when it makes too large an angle (α) with the wall (or line of symmetry), there is no solution for the angle and strength of the reflected shock, so that the "regular" reflection scheme becomes an impossible proposition. In this situation, the actual flow is found to be experimentally following a scheme, as illustrated in Fig. 5, a third shock, namely, the Mach stem (MS) also appears. The Mach stem is frequently curved, and also the reflected shock (RS) is often curved near the triple-shock intersection. Besides the three shock waves, a slip surface (SS) also emanates from the triple point T and separates the streams passing through MS and the two shocks (IS and RS). It is also important to mention here that the liquid height must be continuous across SS, since it is not a shock. However, the loss in energy of the fluid is more in case it passes through a single large shock compared to that when it passes through two smaller shocks with the same total change in height. Accordingly, the fluid velocity is expected to be less downstream of the surface SS than at its upstream. Typical hydraulic jumps analogous to Mach reflection are depicted in Figs. 5(b) and 5(c). The incident shock, reflected shock, Mach stem, and slip surfaces corresponding to Mach reflection are clearly observed. Jumps analogous to both straight and curved Mach stems can be seen. These jumps are observed to occur at relatively higher jet inclination angles and relatively lower jet velocities.

D. Analogies with twin colliding jets

Although the irregular shaped hydraulic jump profiles with single oblique impinging jets have been observed during our experiments, analogous thin liquid sheet profiles have been identified by other researchers as well, during their experimentations with two colliding jets. In some recent studies [28,29], it has been reported that when the two interacting jets are oriented with low angles of obliquity, teardrop or leaf-shaped hydraulic jump profiles can be formed. Interestingly, such patterns have been observed in the present study even with single impinging jets. To elucidate the similarity in the mechanisms of formation of such irregular-

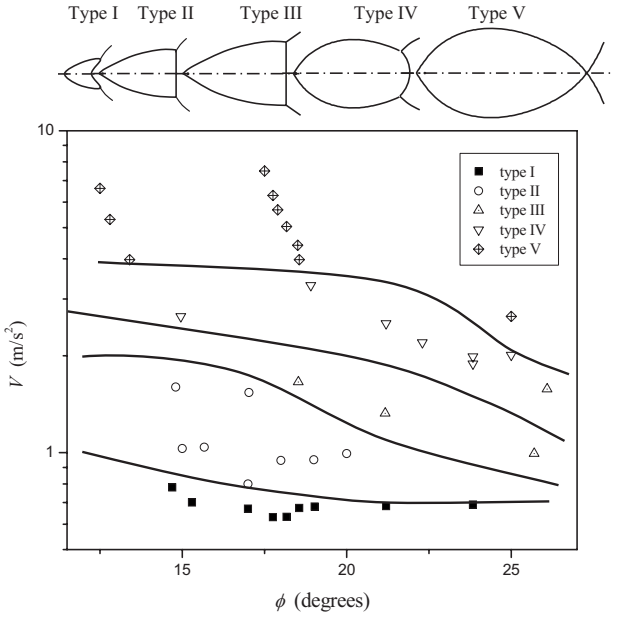

FIG. 7. A phase diagram for hydraulic jumps with corners in the presence of jump-jet interaction with single impinging jets.

shaped jump profiles with single and multiple interacting jets, we have performed a distinct set of experiments with twin jets impinging over one another. An interesting phenomenon could be observed during these experiments, when the centers of the two colliding jets were adjusted to be offset relative to each other. In such a situation, only a portion of two jets (as explained by the two sectional views depicted in Fig. 6) is responsible for the thin film formation, and the film is triangular in shape. The unaffected portions of the two jets form two thick rims, which constitute the two sides of the triangle.

It is interesting to note in this context that when a low velocity liquid jet impinges on the target plate, the back portion [marked L in Fig. 5(a) or in the vicinity of point P in Fig. 5(b)] of it plunges within a thicker liquid pool. Part of the jet mingles with the liquid pool and loses much of its kinetic energy. This portion of the free jet does not take any effective role in forming the thin liquid film. Only the front portion of the jet [marked H in Fig. 5(a)] experiences a drastic change in the momentum. As a result, the direction of flow changes and a shooting flow emanates from the jet, as has been observed in the other cases of jet impingement. However, a thin film does not flow throughout the periphery of the jet; it forms only from the front portion. This gives rise to the triangular pattern, with the jet at the apex of the triangle.

The similarity between Figs. 5(b) and Fig. 6(a) is remarkable. In the case of single impinging jets with typical combinations of low jet velocities and relatively high jet obliquities, the impinging jet plunges into a pool of liquid of relatively higher thickness in the vicinity of $\theta=0$. The shaded portion of the low velocity liquid jet [marked L in Fig. 5(a)] readily mixes with the surrounding liquid pool. Only a part of the circular jet [marked H in Fig. 5(a)] forms the thin film, which flows out radially through a triangular area. Analogous physical behavior can be expected in the case of two interacting free jets as well. In both cases, only a portion of the jet is responsible for the formation of such patterns.

III. SUMMARY

A phase diagram summarizing the indicative regions of the formation of irregular-shaped hydraulic jump profiles, analogous to the regular reflection and Mach reflection waves, is depicted in Fig. 7, for our experiments with single impinging jets. During our studies, it has been observed that hydraulic jumps analogous to regular reflection waves are formed at relatively lower jet inclination angles and higher jet velocities. A transition to Mach reflection-type hydraulic jump profiles has been observed to take place as the jet inclination angle is progressively increased or the jet velocity is progressively reduced.

[1] K. Yokoi and F. Xiao, Physica D **161**, 202 (2002).
[2] S. T. Hansen, S. Hørlück, D. Zauner, P. Dimon, C. Ellegaard, and S. C. Creagh, Phys. Rev. E **55**, 7048 (1997).
[3] T. Bohr, P. Dimon, and V. Putkaradge, J. Fluid Mech. **254**, 635 (1993).
[4] F. J. Higuera, J. Fluid Mech. **274**, 69 (1994).
[5] R. G. Olsson and E. T. Turkdogan, Nature (London) **211**, 813 (1966).
[6] A. D. D. Craik, R. C. Latham, M. J. Fawkes, and P. W. F. Gribbon, J. Fluid Mech. **112**, 347 (1981).
[7] E. J. Watson, J. Fluid Mech. **20**, 481 (1964).
[8] V. E. Nakoryakov, B. G. Pokusaev, and E. N. Troyan, Int. J. Heat Mass Transfer **21**, 1175 (1978).
[9] R. P. Godwin, Am. J. Phys. **61**, 829 (1993).
[10] B. L. Blackford, Am. J. Phys. **64**, 164 (1996).
[11] Y. Brechet and Z. Nèda, Am. J. Phys. **67**, 723 (1999).
[12] S. Watanabe, V. Putkaradze, and T. Bohr, J. Fluid Mech. **480**, 233 (2003).
[13] J. W. M. Bush and J. Aristoff, J. Fluid Mech. **489**, 229 (2003).
[14] C. Ellegaard, A. E. Hansen, A. Haaning, K. Hansen, A. Marcussen, T. Bohr, J. L. Hansen, and S. Watanabe, Nature (London) **392**, 767 (1998); Nonlinearity **12**, 1 (1999).
[15] V. Putkaradze and P. Dimon, Phys. Fluids **12**, 66 (2000).
[16] J. M. Aristoff, J. D. Leblanc, A. E. Hosoi, and J. W. M. Bush, Phys. Fluids **16**, S4 (2004).
[17] J. W. M. Bush, J. Aristoff, and A. E. Hosoi, J. Fluid Mech. **558**, 33 (2006).
[18] S. Beltos, J. Hydraul. Res. **14**, 17 (1976).
[19] A. Rubel, AIAA J. **20**, 1756 (1982).
[20] E. M. Sparrow and B. J. Lovell, J. Heat Transfer **102**, 202 (1980).
[21] J. Stevens and B. W. Webb, Int. J. Heat Mass Transfer **34**, 1227 (1991).
[22] A. Y. Tong, Int. J. Heat Mass Transfer **46**, 2077 (2003).
[23] R. P. Kate, P. K. Das, and S. Chakraborty, J. Fluid Mech. **573**, 247 (2007).
[24] G. I. Taylor, Proc. R. Soc. London, Ser. A **253**, 296 (1959); **253**, 313 (1959); **259**, 1 (1960).
[25] K. D. Miller, J. Appl. Phys. **31**, 1132 (1960).
[26] D. Hasson and R. E. Peck., AIChE J. **10**, 752 (1964).
[27] Y. J. Choo and B. S. Kong, Phys. Fluids **31**, 56 (2001); Y. J. Choo and B. S. Kong, Phys. Fluids **14**, 622 (2002).
[28] J. W. M. Bush and A. E. Hasha, J. Fluid Mech. **54**, 285 (2004).
[29] N. Bremond and E. Villermaux, J. Fluid Mech. **549**, 273 (2006).
[30] P. Krechi and M. Van der Geest, Shock Waves **1**, 3 (1991).
[31] F. R. Gilmore, M. S. Plesset, and H. E. Crossley Jr., J. Appl. Phys. **21**, 243 (1950).
[32] K. M. Hákonardóttir and J. A. Hogg, Phys. Fluids **17**, 077101 (2005).
[33] E. C. Rericha, Ph.D. thesis, University of Texas at Austin, Austin, 2004.